



get for azimuthal field components for  $\rho|s| \gg 1$  at the inner side of the outer surface [13]:

$$H_{\varphi\omega}^{a-} = \frac{q\omega \exp(ik_0 z_0/\beta + i\rho_0 s - 3\pi i/4)}{i\pi v^2 \gamma^2} \sqrt{\frac{2}{\pi \rho_0 s}} \times \frac{ik_0}{s^2} \left\{ -\varepsilon s I_0(r_0 \sigma_0) \tilde{A}_0^{(E2)} + 2 \sum_{\nu=1}^{\infty} I_{\nu}(r_0 \sigma_0) e^{\frac{i\pi(1-\nu)}{2}} \times \right. \quad (3)$$

$$\left. \times \cos(\nu\varphi) \left[ \varepsilon \tilde{A}_{\nu}^{(E2)} \left( is - \frac{1}{2\rho_0} \right) - \frac{i\nu}{\beta \rho_0} \tilde{A}_{\nu}^{(H2)} \right] \right\},$$

$$E_{\varphi\omega}^{a-} = \frac{q\omega \exp(ik_0 z_0/\beta + i\rho_0 s - 3\pi i/4)}{i\pi v^2 \gamma^2} \sqrt{\frac{2}{\pi \rho_0 s}} \times \frac{ik_0}{s^2} 2 \sum_{\nu=1}^{\infty} I_{\nu}(r_0 \sigma_0) e^{\frac{i\pi(1-\nu)}{2}} \times \quad (4)$$

$$\times \sin(\nu\varphi) \left[ i \tilde{A}_{\nu}^{(H2)} \left( is - \frac{1}{2\rho_0} \right) - \frac{\nu}{\beta \rho_0} \tilde{A}_{\nu}^{(E2)} \right],$$

where  $s^2 = k_0^2 \beta^{-2} (\varepsilon \beta^2 - 1)$ ,  $s = \sqrt{s^2}$ ,  $\text{Im}\sqrt{\cdot} > 0$ ,  $\sigma_0^2 = k_0^2 \beta^{-2} (1 - \beta^2)$ ,  $\sigma_0 = \sqrt{\sigma_0^2}$ ,  $\text{Re}\sqrt{\cdot} > 0$ ,  $I_{\nu}$  is a modified Bessel function,  $\gamma$  is a Lorentz factor,  $\tilde{A}_{\nu}^{(E2)}$  and  $\tilde{A}_{\nu}^{(H2)}$  are coefficients determined from linear system based on boundary conditions for  $\rho = a$  (see [13] for details). Component  $H_{\varphi\omega}$  determines ‘‘parallel’’ polarization ( $\parallel$ ) containing components  $E_{z\omega}$ ,  $E_{\rho\omega}$  and  $H_{\varphi\omega}$  with corresponding Fresnel coefficient

$$T_{\parallel} = 2 \cos \theta_i (\cos \theta_i + \sqrt{\varepsilon} \cos \theta_t)^{-1}.$$

Component  $E_{\varphi\omega}$  determines ‘‘orthogonal’’ polarization ( $\perp$ ) containing components  $H_{z\omega}$ ,  $H_{\rho\omega}$  and  $E_{\varphi\omega}$  with corresponding Fresnel coefficient

$$T_{\perp} = 2\sqrt{\varepsilon} \cos \theta_i (\sqrt{\varepsilon} \cos \theta_i + \cos \theta_t)^{-1}.$$

Angle of incidence  $\theta_i$  can be obtained from Snell’s law  $\sqrt{\varepsilon} \sin \theta_i = \sin \theta_t$  and angle of refraction  $\theta_t$ :

$$\sin \theta_t = \frac{-1}{\beta \sqrt{r^2 + r'^2}} \left[ r \sin \theta - r' \cos \theta - \sqrt{\varepsilon \beta^2 - 1} (r \cos \theta + r' \sin \theta) \right], \quad r' = dr/d\theta.$$

Unit vector of transmitted wave  $\vec{e}_k$  is

$$e_{k\rho} = n_{\rho} \cos \theta_t - n_z \sin \theta_t, \quad e_{kz} = n_{\rho} \sin \theta_t + n_z \cos \theta_t.$$

Transmitted fields at the outer surface of the aperture are:

$$H_{\varphi\omega}^a = T_{\parallel} H_{\varphi\omega}^{a-}, \quad \vec{E}_{\omega}^{\parallel} = H_{\varphi\omega}^a [\vec{e}_{\varphi}, \vec{e}_k],$$

$$E_{\varphi\omega}^a = T_{\perp} E_{\varphi\omega}^{a-}, \quad \vec{H}_{\omega}^{\perp} = E_{\varphi\omega}^a [\vec{e}_k, \vec{e}_{\varphi}],$$

$$E_{\rho\omega}^a = H_{\varphi\omega}^a e_{kz}, \quad E_{z\omega}^a = -H_{\varphi\omega}^a e_{k\rho},$$

$$H_{\rho\omega}^a = -E_{\varphi\omega}^a e_{kz}, \quad H_{z\omega}^a = E_{\varphi\omega}^a e_{k\rho}.$$

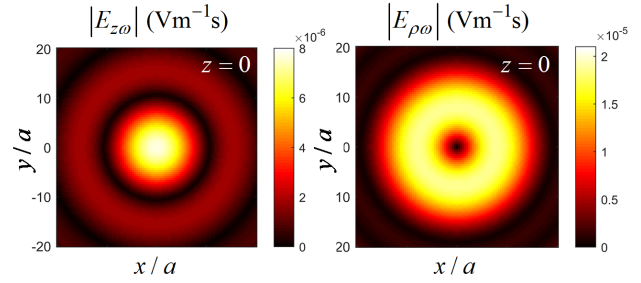


Figure 2: Two dimensional distribution of absolute values of  $E_{z\omega}$  and  $E_{\rho\omega}$  over  $xy$ -plane for symmetrical case  $r_0 = 0$ . in the focal plane.

## NUMERICAL RESULTS

For evaluation of integrals (2), a numerical code was realized in MATLAB with the use of Parallel Computing Toolbox. Parameters for calculations are:  $\omega = 2\pi \cdot 100$  GHz,  $\beta = 0.8$ ,  $f = 500c/\omega$ ,  $z_f = 0$ ,  $q = 1$  nC,  $\varphi_0 = 0$ ,  $x_{\max} = 500c/\omega$ ,  $x_{\max}^{\text{eff}} = 340c/\omega$ ,  $a = c/\omega$ ,  $\theta_{\min} = 162^\circ$ ,  $\theta_{\max} = 179^\circ$ ,  $\varepsilon = 1.6$ ,  $\alpha = 80^\circ$ ,  $\alpha_{\text{tar}} = 73^\circ$ . We will restrict ourselves by taking into account only three modes in Eqs. (3) and (4) which is enough up to  $r_0 = a/2$ .

Figure 2 shows two-dimensional distribution of longitudinal ( $E_{z\omega}$ ) and transverse ( $E_{\rho\omega}$ ) components over  $xy$ -plane for  $z = 0$  and symmetric case  $r_0 = 0$ . As one can clearly see, transverse field is exact zero on the symmetry axis while longitudinal field is maximal here. Transverse field quickly increases with observation point shift from  $z$ -axis and has its maximum value around two times larger compared to maximum of  $E_{z\omega}$ . Total field is practically determined by transverse field excluding small central area.

The case with a shifted charge is shown in Fig. 3. Magnitudes of transverse and longitudinal fields differ approximately by factor 5 and increase almost linearly with increasing  $r_0$ . The most interesting feature is occurred in longitudinal field. For relatively small offset ( $r_0 = a/10$ ), this field is strongly asymmetric with respect to  $x = 0$ . The stronger peak is located in the area  $x > 0$ , i.e. in the area where shifted charge propagates (recall that a charge is shifted to positive  $x$ ). With an increase in  $r_0$  these peaks become more symmetrical ( $r_0 = a/4$ ), and for relatively large offset ( $r_0 = a/2$ ) we have two almost symmetrical peaks located approximately at  $x = 6.7a$  and  $x = -8.7a$ , i.e. far enough from the charge trajectory. More detailed position of the discussed peaks is shown in Fig. 4. In turn, transverse field also has an essential asymmetry for relatively small offset. It is worth noting that the peak of transverse field is shifted in opposite direction compared to the shift of the charge trajectory, its approximate location is  $x = -2.3a$  (see Fig. 4 for details). For larger offsets, the peak of  $E_{\rho\omega}$  becomes practically symmetric in both  $x$  and  $y$  direction, is located nearly in the center and dominates the longitudinal peak.

Possible applications of the presented dielectric concentrator would lie in the area of beam diagnostics and beam manipulation. Since strong field concentration takes place

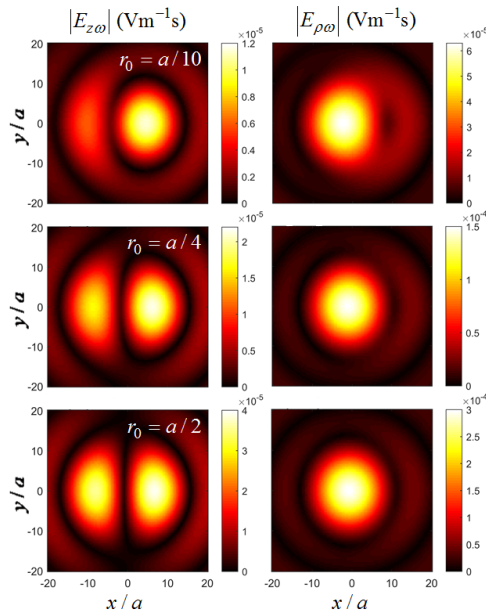


Figure 3: Two dimensional distribution of absolute values of  $E_{z\omega}$  and  $E_{\rho\omega}$  over  $xy$ -plane in the focal plane for  $r_0 = a/10, a/4, a/2$ .

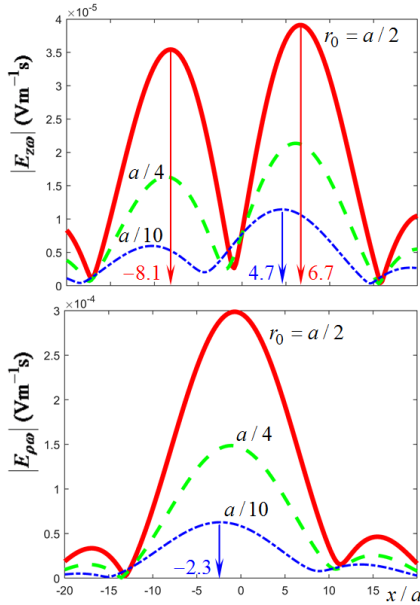


Figure 4: Dependence of absolute values  $E_{z\omega}$  and  $E_{\rho\omega}$  on  $x$  for  $y = z = 0$  and  $r_0 = a/10, a/4, a/2$ .

in the focal plane near the focal point, sensitivity and accuracy of mentioned diagnostics can be essentially increased. For example, peculiarities of field distribution for  $r_0 \neq 0$  can be used for determination of beam shift and positioning the beam to the axis of the structure. Note that difference between magnitudes of two peaks of top plot in Fig. 4 depends on  $r_0$ . For  $r_0 = a/10$ , left peak magnitude is about

50% of the right peak magnitude while for  $r_0 = a/2$  left peak magnitude is about 90% of the right peak magnitude. Moreover, these peaks are shifted for several values of  $a$  (in our case from  $\approx 5$  to  $\approx 8$ ) from the axis thus simplifying the detection of the field.

If the bunch is well aligned along the axis ( $r_0 = 0$ ), it experiences influence of longitudinal field ( $E_{z\omega}$ ) only, see Fig. 2. Interaction between the bunch and strongly concentrated radiated field can lead to longitudinal modulation of the bunch. If the bunch is shifted ( $r_0 \neq 0$ ), it is affected by strong transverse field in the focal plane. Therefore, the concentrator can operate as all-dielectric transverse kicker in this case.

## REFERENCES

- [1] C. Jing, S. Antipov, M. Conde, W. Gai, G. Ha, W. Liu, N. Neveu, J. Power, J. Qiu, J. Shi, D. Wang, and E. Wisniewski, *Nucl. Instrum. Meth. Phys. Res. A*, vol. 898, p. 72, 2018.
- [2] B.D. O'Shea, G. Andonian, S. Barber, K. Fitzmorris, S. Hakimi, J. Harrison, P.D. Hoang, M.J. Hogan, B. Naranjo, O.B. Williams, V. Yakimenko, and J. Rosenzweig, *Nat. Communications*, vol. 7, p. 12763, 2016.
- [3] D. Wang, X. Su, L. Yan, Y. Du, Q. Tian, Y. Liang, L. Niu, W. Huang, W. Gai, C. Tang, and S. Antipov, *Appl. Phys. Lett.*, vol. 111, p. 174102, 2017.
- [4] N. Sei and T. Takahashi, *Scientific Rep.*, vol. 7, p. 17440, 2017.
- [5] A.P. Potylitsyn, S.Y. Gogolev, D.V. Karlovets, G.A. Naumenko, Y.A. Popov, M.V. Shevelev, and L.G. Sukhikh, "Coherent Cherenkov Radiation from a Short bunch Passing near a Target and Possibility of a Bunch Length Diagnostics", in *Proc. IPAC'10*, Kyoto, Japan, May 2010, paper MOPE046, pp. 1074–1076.
- [6] R. Kieffer, L. Bartnik, M. Bergamaschi, V.V. Bleko, M. Billing, L. Bobb, J. Conway, M. Forster, P. Karataev, A.S. Konkov, R.O. Jones, T. Lefevre, J.S. Markova, S. Mazzoni, Y. Padilla Fuentes, A.P. Potylitsyn, J. Shanks, and S. Wang, *Phys. Rev. Lett.*, vol. 121, p. 054802, 2018.
- [7] S.N. Galyamin, A.V. Tyukhtin, and V.V. Vorobev, *J. Instrumentation*, vol. 13, C02029, 2018.
- [8] A.V. Tyukhtin, S.N. Galyamin, and V.V. Vorobev, *Phys. Rev. A*, vol. 99, p. 023810, 2019.
- [9] A.V. Tyukhtin, V.V. Vorobev, S.N. Galyamin, and E.S. Belonogaya, *Phys. Rev. Accel. Beams*, vol. 22, p. 012802, 2019.
- [10] S.N. Galyamin and A.V. Tyukhtin, *Phys. Rev. Lett.*, vol. 113, p. 064802, 2014.
- [11] S.N. Galyamin, A.V. Tyukhtin, and V.V. Vorobev, *Nucl. Instrum. Meth. Phys. Res. B*, vol. 402, p. 144, 2017.
- [12] A.Z. Fradin, *Microwave Antennas*, Pergamon, 1961.
- [13] S.N. Galyamin, V.V. Vorobev and A.V. Tyukhtin, arXiv: 1904.05188, 2019.